PERGAMON

International Journal of Heat and Mass Transfer 45 (2002) 2829–2842

International Journal of HEAT and MASS TRANSFER

www.elsevier.com/locate/ijhmt

Technical Note

Theoretical analysis of film condensation heat transfer inside vertical mini triangular channels

T.S. Zhao [a,*], Q. Liao [b]

[a] *Department of Mechanical Engineering, The Hong Kong University of Sciences and Technology, Clear Water Bay, Kowloon, Hong Kong*

[b] *Institute of Engineering Thermophysics, Chongqing University, Chongqing, China*

Received 6 September 2001; received in revised form 16 October 2001

Abstract

An analytical model is presented for predicting film condensation of vapor flowing inside a vertical mini triangular channel. The concurrent liquid–vapor two-phase flow field is divided into three zones: the thin liquid film flow on the sidewall, the condensate flow in the corners, and the vapor core flow in the center. The model takes into account the effects of capillary force induced by the free liquid film curvature variation, interfacial shear stress, interfacial thermal resistance, gravity, axial pressure gradient, and saturation temperatures. The axial variation of the cross-sectional average heat transfer coefficient of steam condensing inside an equilateral triangular channel is found to be substantially higher than that inside a round tube having the same hydraulic diameter, in particular in the entry region. This enhancement is attributed to the extremely thin liquid film on the sidewall that results from the liquid flow toward the channel corners due to surface tension. The influences of the inlet vapor flow rates, the inlet subcooling, and the channel size on the heat transfer coefficients are also examined.

1. Introduction

Recently, a new type of ultracompact condenser made of a number of parallel, multiport, miniaturized non-circular channels with hydraulic diameter of 0.3 mm $\leqslant D_h \leqslant$ 2.0 mm situated between louvered air-side fins has been developed [1]. The striking feature of this novel condenser is that the condensation heat transfer rate is very high and thus extremely compact. It has been reported that at the same heat transfer rate and the same pressure drop, the volume and weight of this new condenser can be reduced to half of the conventional round tube condenser [1]. Two possible reasons might be responsible for this heat transfer enhancement: thinning the liquid film thickness due to the meniscus effect induced by the sharp corners of the non-circular channel leads to the reduction in the thermal resistance; the increase of the specific surface area may also result in high heat transfer rates. Our literature survey reveals that relatively few studies have reported on the underlying mechanisms leading to high condensing rates inside non-circular channels although extensive work has been done on condensation inside round tubes oriented vertically or horizontally. In this paper, we consider film condensation heat transfer inside a miniaturized triangular channel with a forced motion of vapor.

Yang and Webb [2] experimentally investigated the heat transfer characteristics of R-12 vapor condensing inside two horizontal extruded aluminum rectangular tubes with and without 0.2 mm high micro-fins. The hydraulic diameter was 2.637 mm for the plain tubes and 1.564 mm for the tubes with the micro-fins. Yang and Webb [3] proposed a semi-empirical model to predict the condensation heat transfer coefficient inside the horizontal micro-fin tube with a small hydraulic diameter. They divided the condensation area on the micro-fin surface into the flooded and the unflooded areas. In the

* Corresponding author. Tel.: +852-2358-8647; fax: +852-2358-1543.

E-mail address: metzhao@ust.hk (T.S. Zhao).

0017-9310/02/$ - see front matter
PII: S0017-9310(01)00354-4

Nomenclature

A	cross-sectional area, m^2
b	width of channel side wall, mm
c_{pl}	specific heat of the liquid, W/kg K
D_h	hydraulic diameter, m
f	friction factor
g	gravity acceleration, m/s^2
$\bar{h}$	overall condensation heat transfer coefficient, W/m^2K
$h(z)$	cross-sectional average condensation heat transfer coefficient, W/m^2 K
$h_c(x,z)$	local condensation heat transfer coefficient in the thin film zone, W/m^2 K
h_{fg}	latent heat, J/kg
$h_i(z)$	cross-sectional average condensation heat transfer coefficient defined by the inlet temperature difference, W/m^2 K
$h_{lm}(z)$	local average condensation heat transfer coefficient in the meniscus zone, W/m^2 K
$h_{lt}(z)$	average condensation heat transfer coefficient in the thin film zone, W/m^2 K
K	curvature of the liquid–vapor interface in the thin film zone, m^{-1}
k_l	thermal conductivity of liquid, W/m K
L	channel length, m
$\dot{m}_i$	local mass flux of liquid condensed at the vapor–liquid interface, kg/s
$\dot{m}''$	mass flow rate of condensate, kg/m s
p_c	capillary force, Pa
p	pressure, Pa
P	wetted perimeter, m
Pr_l	Prandtl number
r_c	meniscus radius of the meniscus zone, m
$r_{c,min}$	minimum meniscus radius at the channel inlet, m
Re	Reynolds number
R_g	gas constant, J/kg K
T	temperature, °C
u	liquid velocity in x axis, m/s
v	liquid velocity in y axis, m/s
w	liquid velocity in z axis, m/s
$\bar{w}$	mean velocity, m/s
x	x axis of coordinate
y	y axis of coordinate
z	z axis of coordinate

Greek symbols

α	corner angle, °
β	dispersion constant, J
δ	liquid film thickness, m
δ_0	liquid film thickness at the middle point of the channel sidewall, m
Δp	pressure drop, Pa
ΔT_i	$T_{si} - T_w$, inlet temperature difference, °C
$\Delta T(z)$	$T_s - T_w$, local temperature difference, °C
Φ_l	two-phase frictional pressure drop multiplier
γ	accommodation coefficient
μ	dynamic viscosity, N s/m^2
η_e	coordinate at the end of the thin film zone, m
ρ_l	liquid density, kg/m^3
ρ_v	vapor density, kg/m^3
σ_l	surface tension, N/m
τ_i	interfacial shear stress, N/m^2
τ_{lw}	liquid wall shear stress, N/m^2

Subscripts

e	end of the thin film region
i	inlet or interface
l	liquid
ls	superficial quantities of condensate flow in channel
lv	vapor–liquid two-phase flow
m	meniscus region
s	saturation state
t	thin film region
v	vapor
w	channel wall
Δ	entire channel

flooded area, condensation heat transfer was dominated by vapor shear stress, whereas in the unflooded area, it was dominated by vapor shear stress and surface tension. Using the equivalent mass velocity by Akers et al. [4] and the heat–momentum analogy, Yang and Webb proposed a semi-empirical model incorporating the heat transfer mechanisms in the individual areas, their prediction was in good agreement with the experimental data, with the relative difference being within ±20% [3]. However, the empirical constants used in the model had to be obtained from experiments. Wang and Du [5] proposed an analytical model and conducted experiments to flow condensation on the outside surface of a mini diameter tube in a horizontal annulus, they found that the surface tension effect on condensation heat transfer could not be neglected in the mini tubes having outside diameters less than 3.0 mm, especially at low vapor quality. Nozu and Honda [6] investigated experimentally the condensation of refrigerants in horizontal tubes with spirally grooved microfins and developed a laminar film condensation model in the annular regime. Their model includes the combined effects of the surface tension and vapor shear forces acting on the condensate surface.

The effect of surface tension on the external film condensation on horizontal or vertical finned surfaces has been extensively investigated [7–11]. Karkhu et al. [7] and Rifert et al. [8] analyzed the effect of surface tension on film condensation on finely finned horizontal tubes by assuming that the pressure gradient caused by the surface tension was constant along the surface of the fins. Without using the assumption of constant surface tension, Hirasawa et al. [9] theoretically investigated film condensation on a vertical finned surface and showed that the liquid film near the bottom of a narrow trough became locally thin due to the suction of the liquid flowing into the trough, the predicted liquid film profile was experimentally verified by their optical measurements. Mori et al. [10] theoretically investigated the optimal finned vertical tubular condensers where vapor condenses on the outside surfaces of the tubes. Admak and Webb [11] took account of the local thin film distribution in their analyses of condensation heat transfer on vertical finned plates. Generally, the vapor shear stress was not taken into consideration in the previous investigations of condensation heat transfer on the finned surfaces.

Condensation heat transfer processes inside non-circular miniaturized channels has been also encountered in the condensing sections of micro heat pipes [12–14]. Khrustalev and Faghri [12] developed a mathematical model to calculate the thermal performance of a polygonal micro heat pipe, condensate in the thin film region flows toward the meniscus region under the influence of the surface tension; which means the influence of the interfacial shear stress being neglected, and the accumulated condensate in the meniscus region is drained toward the evaporating section by the capillary force. More recently, Zhang and Faghri [13] numerically investigated condensation at the liquid–vapor meniscus in a capillary grooved channel, the volume of fluid model (VOF) was used to predict the film condensation on the fin top, the condensation at the liquid–vapor meniscus, and the fluid flow in the capillary groove. Thomas et al. [14] studied the flow behaviors of liquid film in a fully developed laminar isothermal flow in a groove with a trapezoidal cross-section, a finite difference solution was employed to determine the mean velocity, volumetric flow rate, and Poiseuille number as functions of the groove aspect ratio, the groove-half angle, and the meniscus contact angle that imposed shear stress at the liquid–vapor interface.

In this work, we report on a theoretical investigation of film condensation heat transfer inside a vertical micro triangular channel, in which the downflow of vapor is driven by a superimposed pressure gradient. The model considers the effects of capillary force induced by the free liquid film curvature variation, interfacial shear stress, interfacial thermal resistance, gravity, axial pressure gradient, and saturation temperatures. It is found that the cross-sectional average heat transfer coefficient of steam condensing inside an triangular channel is significantly higher than that inside a round tube with the same hydraulic diameter, particularly in the entry region. This enhancement is attributed to the extremely thin liquid film on the sidewall resulting from the capillary pressure generated in the channel corners. The influences of the inlet vapor flow rates, the inlet subcooling, and the channel size on the heat transfer coefficients are also discussed.

2. Mathematical model

Consider the film condensation for vapor flowing downward inside a vertical micro equilateral triangular channel with sidewall length b, as illustrated in Fig. 1. Inlet saturated vapor, with temperature of T_{si} at $z = 0$, condenses on the inner surfaces of the channel that is cooled isothermally at a temperature T_w, $(T_w < T_{si})$. The condensate liquid film thickens as it flows to the exit. Because of symmetry, only a one-sixth portion of the cross-section of the equilateral triangular channel needs to be considered, as shown in Fig. 2, the liquid–vapor flow field through the triangular-shaped cross-section is divided into three zones: the thin liquid film zone along the sidewall $(0 \leqslant x \leqslant \eta_e)$, the meniscus zone $(\eta_e < x \leqslant b/2)$ in the corner, and the vapor core zone in the center of the channel. In the thin liquid film zone, part of the condensate produced is drawn into the meniscus zone, in the x-direction, under the influence of the capillary force in the corner, whereas the remaining condensate liquid is drained downward, in the z-direction, due to the gravity and the liquid–vapor interfacial shear stress. In the meniscus zone, the liquid accumulated in the corner is drained downward, in the z-direction, under the influence of both the gravity force and the liquid–vapor interfacial shear stress. The downflow of the vapor in the vapor core zone is due to the externally superimposed pressure gradient. The hydrodynamic interaction between these three flow zones determines the heat transfer rate from the vapor to the channel wall; a simultaneous solution to the hydrodynamics and energy equations in these three flow zones is thus needed for predicting the heat transfer rates.

2.1. Geometric parameters

Referring to Fig. 2, it is assumed that the liquid–vapor interface is tangential to the channel sidewall at the end of the thin film region $(x = \eta_e)$. Thus, the length of the thin film zone, η_e, and the meniscus radius, r_c, are interrelated by

$$\eta_e = \frac{b}{2} - (r_c + \delta_e) ctg\left(\frac{\alpha}{2}\right), \tag{1}$$

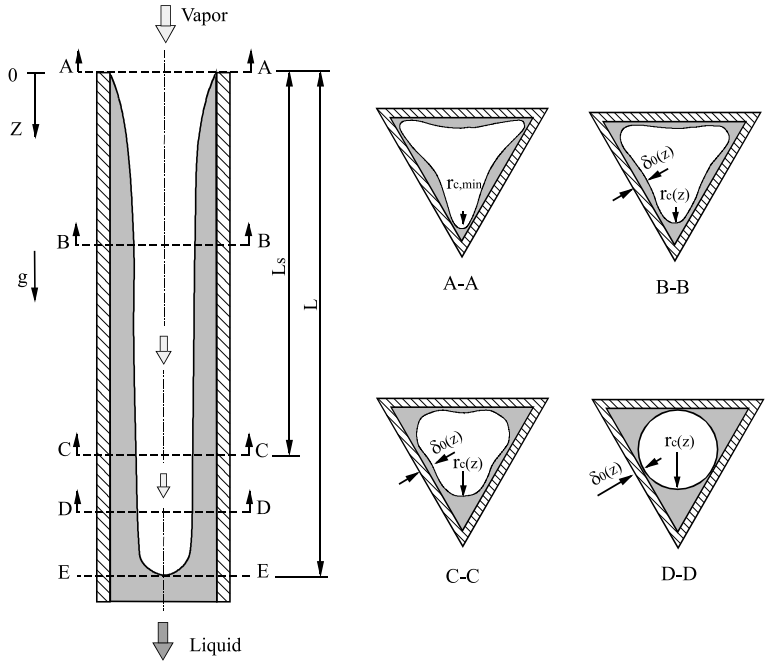

Fig. 1. Schematic of the physical problem.

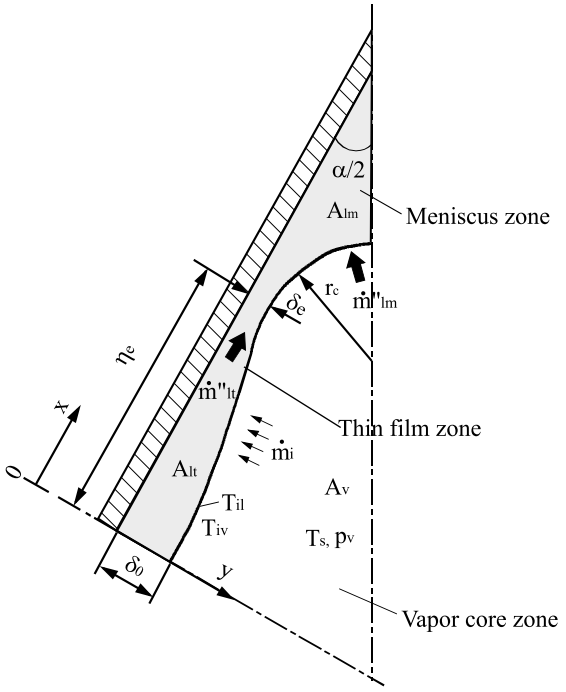

Fig. 2. Illustration of the liquid film profile inside the triangular channel.

where α is the angle of the triangular corner, ($\alpha = \pi/3$ for an equilateral triangular channel), and δ_e is the liquid film thickness at $x = \eta_e$. The cross-sectional areas of the thin liquid film zone, A_{lt}, the meniscus zone, A_{lm}, and the vapor core zone, A_v, are given, respectively, as

$$A_{lt} \doteq 0.5(\delta_e + \delta_0)\eta_e, \tag{2}$$

$$A_{lm} = 0.5\left[(r_c + \delta_e)^2 ctg\left(\frac{\alpha}{2}\right) - \left(\frac{\pi}{2} - \frac{\alpha}{2}\right) r_c^2\right], \tag{3}$$

and

$$A_v = A_\Delta - A_{lt} - A_{lm} = \frac{b^2}{8} tg\frac{\alpha}{2} - A_{lt} - A_{lm}. \tag{4}$$

Here, δ_0 denotes the film thickness at the middle of the sidewall ($x = 0$) and A_Δ is the cross-sectional area of the triangular channel. The hydraulic diameter, D_h, of the entire triangular channel would be

$$D_h = \frac{2}{3} b \sin\alpha, \tag{5}$$

while the hydraulic diameter of the meniscus zone, D_{hl}, and the hydraulic diameter of the vapor core zone, D_{hv}, are given, respectively, as

$$D_{hl} = \frac{4A_{lm}}{P_{lm}} \tag{6}$$

and

$$D_{hv} = \frac{4A_v}{P_v}, \tag{7}$$

where the wetted perimeters of the meniscus zone and the vapor core zone, P_{lm}, and P_v, are represented by

$$P_{\mathrm{lm}} = (r_{\mathrm{c}} + \delta_{\mathrm{e}})ctg\left(\frac{\alpha}{2}\right) \tag{8}$$

and

$$P_{\mathrm{v}} \doteq \left(\frac{\pi}{2} - \frac{\alpha}{2}\right)r_{\mathrm{c}} + \sqrt{\eta_{\mathrm{e}}^2 + (\delta_{\mathrm{e}} - \delta_0)^2}. \tag{9}$$

The liquid–vapor interface perimeter, P_{i}, in the meniscus zone is

$$P_{\mathrm{i}} = \left(\frac{\pi}{2} - \frac{\alpha}{2}\right)r_{\mathrm{c}}. \tag{10}$$

All the geometric parameters are function of η_{e}, δ_{e}, and δ_0, which are associated with both hydrodynamic and heat transport processes in the thin film zone, the meniscus zone, and the vapor core zone.

2.2. Thin liquid film flow ($0 \leqslant x < \eta_e$)

In the thin liquid film zone, assumed the liquid motion being an incompressible, two-dimensional laminar flow with constant fluid properties. It is further assumed that heat transfer across the liquid film is by pure conduction. Then, referring to the coordinates shown in Fig. 2, the simplified governing conservation equations of mass, momentum and energy in the thin film zone ($0 \leqslant x < \eta_{\mathrm{e}}$) can be written as

$$\frac{\partial u}{\partial x} + \frac{\partial v}{\partial y} + \frac{\partial w}{\partial z} = 0, \tag{11}$$

$$\mu_{\mathrm{l}}\frac{\partial^2 u}{\partial y^2} - \frac{\partial p_{\mathrm{lt}}}{\partial x} = 0, \tag{12}$$

$$\mu_{\mathrm{l}}\frac{\partial^2 w}{\partial y^2} - \frac{\partial p_{\mathrm{lt}}}{\partial z} + \rho_{\mathrm{l}}g = 0, \tag{13}$$

and

$$\frac{\partial^2 T_{\mathrm{lt}}}{\partial y^2} = 0, \tag{14}$$

where the subscript "lt" represent the quantities in the thin film zone and δ is the thickness of liquid film normal to the channel wall in the thin film zone. The other symbols are listed in the Nomenclature. The pressure of condensate, p_{lt}, in the thin film zone is related to the vapor pressure by the Young–Laplace equation, i.e.

$$\frac{\partial p_{\mathrm{lt}}}{\partial x} = \frac{\partial}{\partial x}\left(p_{\mathrm{v}} - \frac{\sigma_{\mathrm{l}}}{r_{\mathrm{l}}}\right), \tag{15}$$

where σ_{l} is the surface tension and

$$r_{\mathrm{l}} = \frac{[1 + (\partial\delta/\partial x)^2]^{3/2}}{\partial^2\delta/\partial x^2}$$

is the liquid–vapor interface curvature radius. Assuming that the vapor pressure, p_{v}, is constant across the vapor core zone ($\partial p_{\mathrm{v}}/\partial x = 0$) allows us to modify Eq. (15) as

$$\frac{\partial p_{\mathrm{lt}}}{\partial x} = -\sigma_{\mathrm{l}}\frac{\partial}{\partial x}\left\{\frac{(\partial^2\delta/\partial x^2)}{[1 + (\partial\delta/\partial x)^2]^{3/2}}\right\}. \tag{16}$$

On the inner surface of the channel wall ($y = 0$), the boundary conditions are

$$u = 0, \quad w = 0, \tag{17a}$$

$$T_{\mathrm{lt}} = T_{\mathrm{w}}. \tag{17b}$$

At the liquid–vapor interface ($y = \delta$), they are

$$\frac{\partial u}{\partial y} = 0, \quad \mu_{\mathrm{l}}\frac{\partial w}{\partial y} = \tau_{\mathrm{i}}, \tag{18a}$$

$$T_{\mathrm{lt}} = T_{\mathrm{il}}, \quad \dot{m}_{\mathrm{i}}h_{\mathrm{fg}} = k_{\mathrm{l}}\frac{\partial T_{\mathrm{lt}}}{\partial y}, \tag{18b}$$

where τ_{i}, $\dot{m}_{\mathrm{i}}$, and T_{il} are the shear stress, the condensing mass flux, and the local interfacial liquid temperature at the liquid–vapor interface, respectively; k_{l} is the thermal conductivity and h_{fg} is the latent heat of the liquid.

Combining Eqs. (12) and (16) to eliminate the pressure gradient term and performing integration subject to the boundary conditions (17a) and (18a) across the film thickness yields

$$u = \left[(y/\delta) - \frac{1}{2}(y/\delta)^2\right]\frac{\sigma_{\mathrm{l}}\delta^2}{\mu_{\mathrm{l}}} \times \frac{\partial}{\partial x}\left\{\frac{(\partial^2\delta/\partial x^2)}{[1 + (\partial\delta/\partial x)^2]^{3/2}}\right\}. \tag{19}$$

Similarly, integrating equation (13) subject to the boundary conditions (17a) and (18a) gives

$$w = \left\{\left(\frac{\partial p_{\mathrm{lt}}}{\partial z} - \rho_{\mathrm{l}}g\right)\frac{y^2}{2} + \left[\tau_{\mathrm{i}} - \left(\frac{\partial p_{\mathrm{lt}}}{\partial z} - \rho_{\mathrm{l}}g\right)\delta\right]y\right\}\Big/\mu_{\mathrm{l}}. \tag{20}$$

The small variation of the liquid film curvature along the z-direction in the mini channel may allow us to neglect the effect of the capillary force on the liquid pressure gradient, $\partial p_{\mathrm{lt}}/\partial z$, to give

$$\frac{\partial p_{\mathrm{lt}}}{\partial z} = \frac{\mathrm{d}p_{\mathrm{v}}}{\mathrm{d}z}. \tag{21}$$

Combining Eqs. (20) and (21) to eliminate the term $\partial p_{\mathrm{lt}}/\partial z$ yields

$$w = \left\{\left(\frac{\mathrm{d}p_{\mathrm{v}}}{\mathrm{d}z} - \rho_{\mathrm{l}}g\right)\frac{y^2}{2} + \left[\tau_{\mathrm{i}} - \left(\frac{\mathrm{d}p_{\mathrm{v}}}{\mathrm{d}z} - \rho_{\mathrm{l}}g\right)\delta\right]y\right\}\Big/\mu_{\mathrm{l}}. \tag{22}$$

Assuming that the temperature across the liquid film varies linearly and integrating Eq. (14) subject to the boundary conditions (17b) and (18b), we obtain

$$\dot{m}_{\mathrm{i}} = \left(k_{\mathrm{l}}\frac{T_{\mathrm{il}} - T_{\mathrm{w}}}{\delta}\right)\Big/h_{\mathrm{fg}}, \tag{23}$$

where the local condensate mass flux, $\dot{m}_i$, at the liquid–vapor interface can also be obtained by integrating the continuity Eq. (11) across the film thickness, i.e.

$$\dot{m}_i = \rho_l \left[\frac{\partial}{\partial x} \left(\int_0^\delta u \, dy \right) + \frac{\partial}{\partial z} \left(\int_0^\delta w \, dz \right) \right]. \tag{24}$$

The liquid film in the thin film zone is extremely thin such that the interfacial thermal resistance at the liquid–vapor interface should be taken into account [15]. Following the analysis by Stephan and Busse [16], we obtain the interfacial liquid temperature, T_{il}, as

$$T_{il} = T_{iv} - \dot{m}_i h_{fg} \left[\frac{T_s \sqrt{2\pi R_g T_s}}{h_{fg}^2 \rho_v} \frac{(2-\gamma)}{\gamma} \right], \tag{25}$$

where R_g is the gas constant, γ the accommodation coefficient, ρ_v the vapor density and T_s the saturation temperature.

$$T_{iv} = T_s \left(1 + \frac{p_c}{h_{fg} \rho_l} \right) \tag{26}$$

is the local interfacial vapor temperature in the vapor core zone, with the capillary pressure, p_c, represented by

$$p_c = \sigma_l K + \frac{\beta}{\delta^3}, \tag{27}$$

with K being the meniscus curvature of the liquid film and β the dispersion constant with regard to the disjoining force. Substituting Eq. (25) into (23) yields

$$\dot{m}_i = (T_{iv} - T_w) \Bigg/ h_{fg} \left[\frac{\delta}{k_l} + \frac{T_s \sqrt{2\pi R_g T_s}}{h_{fg}^2 \rho_v} \frac{(2-\gamma)}{\gamma} \right]. \tag{28}$$

Inserting Eqs. (19) and (22) for u and w into Eq. (24) and then combining with Eq. (28) to eliminate $\dot{m}_i$, we obtain a partial differential equation for the local film thickness distribution $\delta(x,z)$ in the thin film flow zone as

$$\begin{aligned} &\frac{\sigma_l}{3} \frac{\partial}{\partial x} \left[\delta^3 \frac{\partial}{\partial x} \left\{ \frac{\partial^2 \delta / \partial x^2}{[1 + (\partial \delta / \partial x)^2]^{2/3}} \right\} \right] \\ &\quad + \frac{\partial}{\partial z} \left[\tau_i \frac{\delta^2}{2} - \left(\frac{dp_v}{dz} - \rho_l g \right) \frac{\delta^3}{3} \right] \\ &\quad = \frac{(T_{iv} - T_w)\mu_l}{\rho_l h_{fg}} \Bigg/ \left[\frac{\delta}{k_l} + \frac{T_s \sqrt{2\pi R_g T_s}}{h_{fg}^2 \rho_v} \frac{(2-\gamma)}{\gamma} \right]. \end{aligned} \tag{29}$$

The unknowns dp_v/dz, τ_i, and T_s in Eq. (29) will be obtained by analyzing the hydrodynamic field in the vapor core zone in the later sections. Noting that Eq. (29) is a fourth-order partial differential equation, four boundary conditions are needed. The geometric symmetry of condensate with respect to the middle of the channel sidewall ($x = 0$) gives

$$x = 0: \qquad \frac{\partial \delta}{\partial x} = 0, \quad \frac{\partial^3 \delta}{\partial x^3} = 0. \tag{30}$$

The third boundary condition can be obtained by assuming that the condensate film surface is tangential to the channel sidewall at the end of the thin film region ($x = \eta_e$), i.e.

$$x = \eta_e: \qquad \frac{\partial \delta}{\partial x} = 0, \tag{31}$$

where the thin film zone length, η_e, is associated with the meniscus zone as discussed in the following section. At the channel inlet, $z = 0$, all the condensate is assumed to be drawn into the meniscus zone by the capillary force along the x direction. Therefore, the film thickness $\delta(x,0)$ can be obtained by solving the following equation:

$$\begin{aligned} &\frac{\sigma_l}{3} \frac{d}{dx} \left[\delta^3 \frac{d}{dx} \left\{ \frac{d^2\delta/dx^2}{[1 + (d\delta/dx)^2]^{2/3}} \right\} \right] \\ &\quad = \frac{(T_{iv} - T_w)\mu_l}{\rho_l h_{fg}} \Bigg/ \left[\frac{\delta}{k_l} + \frac{T_s \sqrt{2\pi R_g T_s}}{h_{fg}^2 \rho_v} \frac{(2-\gamma)}{\gamma} \right], \end{aligned} \tag{32}$$

which is obtained by simplifying Eq. (29) at $z = 0$. Eq. (32) is also a fourth-order ordinary differential equation, which can be solved subject to the boundary conditions given by Eqs. (30) and (31), with one more additional boundary condition given by

$$x = \eta_e: \qquad \frac{d^2\delta}{dx^2} = \frac{1}{r_{c,min}}. \tag{33}$$

Eq. (33) represents the liquid–vapor interfacial curvature at the channel inlet, where $r_{c,min}$ denotes the minimum meniscus radius and can be obtained from the corresponding irreducible residual saturation, s_{ir}, inside the capillary channel. The irreducible residual saturation refers to the liquid fraction that resides permanently in the channel corners due to surface tension and is defined as

$$s_{ir} = \frac{A_{l,min}}{A_\Delta}, \tag{34}$$

where $A_{l,min}$ represents the cross-sectional area occupied by the irreducible residual liquid in the channel corners. Following Wang et al. [17] for modeling two-phase flow in mini polygonal channels using the porous medium approach for an equilateral triangular channel, we relate the irreducible residual saturation, s_{ir}, to the minimum meniscus radius, $r_{c,min}$, as

$$s_{ir} = \frac{0.5\left[ctg\left(\frac{\alpha}{2}\right) - \left(\frac{\pi}{2} - \frac{\alpha}{2}\right)\right] r_{c,min}^2}{A_\Delta}. \tag{35}$$

Saez and Carbonell [18] developed a correlation of the irreducible residual saturation for capillary materials as

$$s_{ir} = \frac{1}{20 + 0.9Eö}, \tag{36}$$

where *Eö* represents the *Eötvös* number, defined as

$$E\ddot{o} = \frac{\rho_l g D_h^2}{\sigma_l}. \tag{37}$$

Combining Eqs. (35) and (36) yields the minimum meniscus radius such that the boundary condition given by Eq. (33) is determined. Hence, Eq. (32) can be solved, and subsequently, the film thickness distribution in the thin film zone can now be obtained from Eq. (29) provided that τ_i, T_s, and dp_v/dz are known.

2.3. Accumulated condensate flow ($\eta_e \leqslant x \leqslant b/2$)

In the meniscus zone, it is assumed that the momentum equation for the liquid motion in the corner with cross-sectional area, A_{lm}, is a one-dimensional flow with the inertia term neglected due to the rather small Reynolds numbers in the mini channel. A similar assumption has been adopted extensively by many other investigators [12,19–22] for liquid flow in the condensation section and evaporation section of micro triangular heat pipes. The momentum conservation equation for the liquid flow in the meniscus zone with cross-sectional area, A_{lm}, is given by

$$-\frac{dp_{lm}}{dz} - \frac{\rho_l}{A_{lm}}\frac{d}{dz}\left(\bar{w}_{lm}^2 A_{lm}\right) + \rho_l g + \frac{\tau_i P_i}{A_{lm}} - \frac{\tau_{lw} P_{lm}}{A_{lm}} = 0, \tag{38}$$

where the subscript "lm" represents the quantities in the meniscus zone, τ_{lw} is the liquid-wall shear stress, and $\bar{w}_{lm}$ is the mean liquid velocity in the meniscus zone. In Eq. (38), the second term is usually small to be neglected [12,20]. The liquid-wall shear stress, τ_{lw}, for flow in an equilateral triangular channel can be expressed as [23]

$$\tau_{lw} = \frac{1}{2}\rho_l \bar{w}_{lm}^2 f_l, \tag{39}$$

where $f_l = (13.3/Re_{lm})$ is the friction factor, with Reynolds number defined as $Re_{lm} = (\rho_l \bar{w}_{lm} D_{hl}/\mu_l)$. The liquid pressure gradient, dp_{lm}/dz, in Eq. (38) is related to the vapor pressure gradient, dp_v/dz, by the Young–Laplace equation, as

$$\frac{dp_{lm}}{dz} = \frac{dp_v}{dz} - \frac{d}{dz}\left(\frac{\sigma_l}{r_c}\right). \tag{40}$$

We now obtain the mean liquid velocity in the meniscus zone, $\bar{w}_{lm}$, by considering the mass balance in the meniscus zone. Referring to Fig. 2, the variation of the condensate liquid flow rate in the meniscus zone with the z-direction is due to the condensate liquid rate per unit axial length that enters the meniscus zone, i.e.

$$\rho_l \frac{d(\bar{w}_l A_{ml})}{dz} = \dot{m}''_{lt} + \dot{m}''_{lm}, \tag{41}$$

where

$$\dot{m}''_{lt} = \int_0^{\delta_e} \rho_l u \, dy = \frac{\rho_l \sigma_l \delta_e^3}{3\mu_l}\frac{\partial}{\partial x}\left\{\frac{(\partial^2\delta/\partial x^2)}{[1+(\partial\delta/\partial x)^2]^{3/2}}\right\}\Bigg|_{x=\eta_e} \tag{42}$$

represents the condensate liquid flow that enters the meniscus zone at $x = \eta_e$, and

$$\dot{m}''_{lm} = \frac{(b/2-\eta_e)h_{lm}(z)\Delta T(z)}{h_{fg}} \tag{43}$$

is the condensing mass flux entering the meniscus zone, with $\Delta T(z) = T_s - T_w$ and $h_{lm}(z)$ being the local average condensation heat transfer coefficient in the meniscus zone that will be defined in Section 2.5.

2.4. Vapor core flow

In dealing with the vapor flow in the vapor core zone, we assume: (1) the vapor motion in the vapor core zone being a one-dimensional incompressible fully developed flow; (2) the peripheral condensate liquid being stationary based on the fact that the vapor velocity is usually much higher than the liquid [12,20]; (3) the contribution of the momentum flux due to the phase change at the liquid–vapor interface being neglected. Based on these assumptions, the axial momentum conservation equation for the vapor flow can be taken as

$$-\frac{dp_v}{dz} + \frac{\rho_v}{A_v}\frac{d}{dz}(\bar{w}_v^2 A_v) + \rho_v g + \frac{\tau_i P_v}{A_v} = 0, \tag{44}$$

where $\bar{w}_v$ is the mean velocity of the vapor flow. The liquid–vapor interfacial shear stress, τ_i, is given by

$$\tau_i = \frac{1}{2}\rho_v \bar{w}_v^2 f_v, \tag{45}$$

where the friction factor, f_v, of the vapor flow is

$$f_v = cRe_v^{-m}, \tag{46}$$

with c and m being empirical constants, and the Reynolds number, defined as $Re_v = (\rho_v \bar{w}_v D_{hv}/\mu_v)$. As in [24,25], in the present work, $c = 16$ and $m = 1.0$ are taken for the laminar vapor flow, while $c = 0.046$ and $m = 0.2$ are used for the turbulent flow of vapor.

The mean vapor velocity, $\bar{w}_v$ can be obtained by considering the mass balance of the vapor along the channel length, i.e.

$$\rho_v \frac{d(\bar{w}_v A_v)}{dz} = h(z)(T_s - T_w)b/(2h_{fg}), \tag{47}$$

where $h(z)$ is the average condensation heat transfer coefficient at each cross section along the z axis. Eq. (47) reflects the fact that the reduction of the mass flow rate

of vapor along the z-direction is due to the condensation at the liquid–vapor interface. $\bar{w}_v$, τ_i, and dp_v/dz can be obtained by solving Eqs. (44)–(47) provided that $h(z)$, A_v, and D_{hv} are known. A_v and D_{hv} are related with η_e, δ_e, δ_0, and r_c and can be derived from Eqs. (2)–(4), (7), and (9) while the local average heat transfer coefficient $h_{lm}(z)$ of the meniscus zone and the average heat transfer coefficient, $h(z)$, over the entire cross-section is obtained in the following section.

The local saturation temperature of the vapor in the vapor core region, T_s, is obtained from the Clausius–Clapeyron equation

$$\frac{dp_v}{dT_s} = \frac{\rho_l \rho_v h_{fg}}{(\rho_l - \rho_v) T_s}. \tag{48}$$

2.5. Heat transfer coefficients

The hydrodynamic fields in the peripheral thin liquid film and the relatively thick condensate in the meniscus zone are different from each other. Thus, the heat transfer coefficients in the thin film and the meniscus zones should be treated separately.

In thin film zone, the local heat transfer coefficient, $h_c(x,z)$, is defined as

$$h_c(x,z) = \frac{q''_c(x,z)}{T_s - T_w} = \frac{\dot{m}_i h_{fg}}{T_s - T_w}, \quad 0 \leqslant x < \eta_e, \tag{49}$$

where $q''_c(x,z)$ is the local heat flux at the liquid–vapor interface. Substituting Eq. (28) for $\dot{m}_i$ into Eq. (49) gives

$$h_c(x,z) = \left(\frac{T_{iv} - T_w}{T_s - T_w}\right) \Bigg/ \left[\frac{\delta}{k_l} + \frac{T_s\sqrt{2\pi R_g T_s}}{h_{fg}^2 \rho_v} \frac{(2-\gamma)}{\gamma}\right], \quad 0 \leqslant x < \eta_e. \tag{50}$$

The average heat transfer coefficient, $h_{lt}(z)$, over the thin film zone is then given by

$$h_{lt}(z) = \left[\int_0^{\eta_e} h_c(x,z)\,dx\right] \Big/ \eta_e. \tag{51}$$

The condensate flow in the meniscus zone is quite similar to the accumulated condensate flow at the lower part of the tube for the stratified flow in a horizontal condensing tube. Following the analysis of Chen and Koamustafaogullari [25] on condensation heat transfer of stratified co-current flow in a horizontal tube, the local average heat transfer coefficient, $h_{lm}(z)$, in the meniscus zone is given by

$$h_{lm}(z) = \frac{\Phi_l (k_l/D_h)(8Re_{ls})^{1/2}}{5 + 5[\ln(5Pr_l + 1)]Pr_l^{-1}}, \tag{52}$$

where Pr_l is the Prandtl number of the liquid and $Re_{ls} = (\rho_l \bar{w}_{ls} D_h/\mu_l)$ is the superficial Reynolds number of the condensate flow in the channel, with D_h being the hydraulics diameter of the entire channel cross-section and $\bar{w}_{ls} = (\bar{w}_{lm} A_{lm}/A_\Delta)$ being the superficial velocity of the condensate flow in the channel,

$$\Phi_l = \sqrt{\frac{\Delta p_{lv}}{\Delta p_l}} = \sqrt{\frac{dp_v/dz}{dp_l/dz}}$$

is the square root of the two-phase frictional pressure drop multiplier, with Δp_l representing the pressure drop of the liquid flowing alone in the triangular channel and Δp_{lv} the pressure drop of the two-phase flowing, which is equal to the vapor pressure drop, Δp_v, in the vapor core zone.

The pressure gradient, dp_l/dz, is represented by

$$\frac{dp_l}{dz} = \frac{P_\Delta}{A_\Delta}\tau_l, \tag{53}$$

where the wall shear stress for the liquid flowing alone in the triangular channel can be obtained from Eq. (39) as $\tau_l = (6.65\mu_l \bar{w}_{ls}/D_h)$, subscripts "$\Delta$" refers to entire triangular cross-section. Therefore, the local average heat transfer coefficient in the meniscus zone, $h_{lm}(z)$, can be obtained from Eqs. (52) and (53) provided that $\bar{w}_{lm}$ and A_{lm} are known.

The average condensation heat transfer coefficient $h(z)$ over the entire cross-section is evaluated from

$$h(z) = [\eta_e h_{lt}(z) + (b/2 - \eta_e) h_{lm}(z)]/(b/2). \tag{54}$$

It is clear from Eq. (47) that the average heat transfer coefficient, $h(z)$, over the cross-section given by Eq. (54) is defined based on the local temperature difference, $\Delta T(z) = T_s - T_w$. Alternatively, the average condensation heat transfer coefficient over the cross-section, $h_i(z)$ can also be defined based on the inlet temperature difference, $\Delta T_i = T_{si} - T_w$, with T_{si} being the inlet vapor saturation temperature while $h_i(z)$ is related to $h(z)$ by

$$h_i(z) = [\Delta T(z)/\Delta T_i] h(z). \tag{55}$$

The overall condensation heat transfer coefficient, $\bar{h}$, over the entire channel length is then given by

$$\bar{h} = \left[\int_0^L h_i(z)\,dz\right] \Big/ L, \tag{56}$$

where L represents the channel length.

3. Numerical simulation

3.1. Numerical treatment

The calculation of the local and the average heat transfer coefficient proceeds in a stepwise manner as follows:

(1) Solve Eq. (32) by the fourth-order Runge–Kutta method and obtain the profile of the film thickness at the channel inlet, $z = 0$.

(2) Discretize the terms with the z-derivatives ($\partial/\partial z$) in Eqs. (29), (38), (41), (44), and (47) using the backward finite difference with an increment Δz.
(3) The interfacial shear stress, τ_i, the vapor pressure gradient, dp_v/dz, and local saturation temperature, T_s, based on the inlet conditions or the previous axial position z for the subsequent increments are initially utilized to solve for $\delta(0,z)$ from Eq. (29).
(4) simultaneously solve Eqs. (29), (38) and (41) for $\delta(x,z)$, $h_e(z)$, and $r_c(z)$. Noting that Eq. (29) is reduced to a fourth-order ordinary differential equation with respect to x, when the terms with $\partial/\partial z$ is discretized using the backward finite difference, it can be solved by the fourth-order Runga–Kutta method.
(5) Solve Eqs. (51), (52), and (54) for $h_{lt}(z)$, $h_{lm}(z)$, and $h(z)$.
(6) Obtain the new values of τ_i, dp_v/dz, and T_s by simultaneously solving Eqs. (44), (47) and (48);
(7) repeat steps (3)(4)(5)(6). The iteration process is terminated when the two successive values of η_e agree within a specified tolerance ($\pm 10^{-3}$).
(8) the numerical calculation procedure is haltedwhen $\bar{w}_v A_v = 0$ or if $T_s(z) \leqslant T_w$.

3.2. Results and discussion

Three channels with sidewall lengths of 2.0, 1.5, and 1.0 mm, corresponding to hydraulic diameters of 1.16, 0.87, and 0.58 mm, are considered, as to predict the condensation of the forced downflow of the steam inside the mini vertical equilateral triangular channels. Saturated steam at its saturation temperature (100 °C) corresponding to the standard atmospheric pressure is introduced at the inlet of the channel (Fig. 1). The thermophysics properties of water and steam necessary for calculations are listed in Table 1. Unless otherwise noted, typical results will be presented for the channel with a sidewall length of 2.0 mm under three conditions: Case I, $Re_{vi} = 4500$ and $\Delta T_i = T_{si} - T_w = 6$ °C; Case II, $Re_{vi} = 3000$ and $\Delta T_i = 6$ °C; as well as Case III, $Re_{vi} = 3000$ and $\Delta T_i = 4$ °C.

Table 1
Thermophysical properties of water

Gas constant, R_g	462 (J/kg K)
Dispersion constant, β	2.0×10^{-21} (J)
Accommodation coefficient, γ	0.03
Surface tension, σ_l	0.05886 (N m^{-1})
Latent heat of evaporation, h_{fg}	2257.1×10^3 (J kg^{-1})
Liquid specific heat, c_{pl}	4220 (J kg^{-1} K^{-1})
Density of liquid, ρ_l	958.4 (kg m^{-3})
Density of vapor, ρ_v	0.5977 (kg m^{-3})
Dynamics viscosity of liquid, μ_l	2.825×10^{-4} (N s m^{-2})
Dynamics viscosity of vapor, μ_v	1.202×10^{-5} (N s m^{-2})
Thermal conductivity of liquid, k_l	0.683 (W m^{-1} K^{-1})
Prandtl number of liquid, Pr_l	1.75

3.2.1. Thin liquid film profiles

Fig. 3 presents the liquid film thickness profiles at the selected axial locations ($z = 50$, 100, 150, and 200 mm) for Case I. The liquid film profiles indicate that the thin liquid film zone ($0 \leqslant x \leqslant \eta_e$) occupies the majority of the area of the sidewall although the film thickness increases rapidly when the meniscus zone ($\eta_e \leqslant x \leqslant b/2$) is attained. As the fluid moves progressively toward the downstream, the film thickness in the thin film zone decreases and the meniscus zone enlarges. It is interesting to note that the liquid film in the thin film zone takes a convex-shaped profile over the entire sidewall, with the crest located at the middle of the sidewall (note that the liquid film profile is symmetric and only half of the sidewall is shown in Fig. 3). This particular liquid film profile results from the balance between a pressure gradient generated by the vapor–liquid meniscus interface at the corners of the channel and the resistance against the liquid flow toward the corners. The convex-shaped liquid film profiles predicted in this work are in agreement with the experimental measurements of the liquid film in a vertical small trough by Hirasawa et al. [9].

3.2.2. Heat transfer coefficients

Fig. 4 presents the variation of the local condensation heat transfer coefficients along the sidewall at selected axial distances for Case I. The heat transfer coefficient at each axial distance ($z = 50$, 100, 150, and 200 mm) increases continuously along the sidewall length until the meniscus zone is attained ($x = \eta_e$) and drops immediately to the meniscus zone heat transfer coefficient,

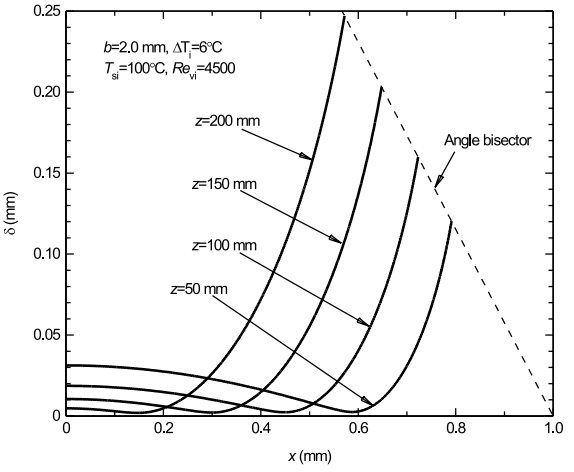

Fig. 3. Profiles of the liquid film thickness along the sidewall at various axial distances.

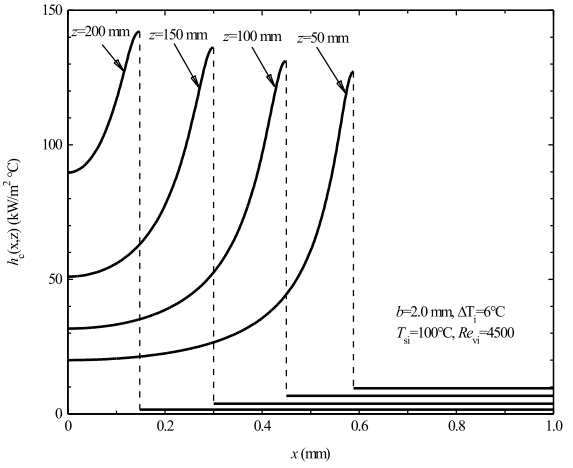

Fig. 4. Variations of the local heat transfer coefficients along the sidewall at selected axial distances.

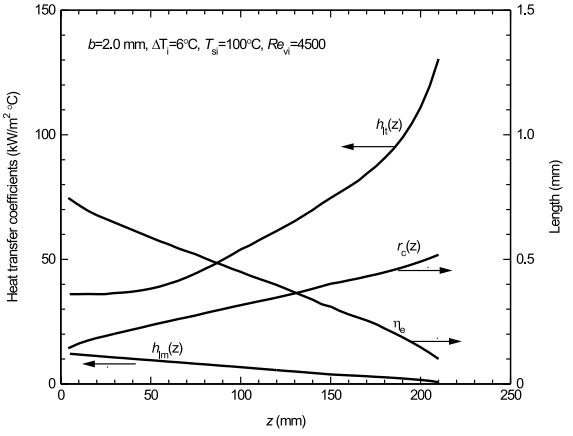

Fig. 5. Variations of the local average heat transfer coefficient, the meniscus radius, and the thin film zone along the axial length.

$h_{lm}(z)$, as given by Eq. (52). It should be recognized, however, that the sudden drop of the heat transfer coefficient between the thin film zone and the meniscus zone is not expected in real situations. It is caused by the mathematical model assuming two condensation zones: the thin film zone $(0 \leqslant x \leqslant \eta_e)$ and the meniscus zone $(\eta_e \leqslant x \leqslant b/2)$. The high heat transfer coefficients in the thin film zone are apparently associated with the thin liquid film presented in Fig. 3. Fig. 4 also indicates that the heat transfer coefficients in the thin film zone are higher than that at downstream locations, while the heat transfer coefficients in the meniscus zone decreased due to enlarging meniscus zone along the axial distance.

Fig. 5 presents the variations of the several key parameters with the axial distance for steam condensing inside the channel with $b = 2.0$ mm under the condition of $Re_{vi} = 4500$ and $\Delta T_i = 6$ °C. The parameters presented in Fig. 5 include the thin film zone width, η_e, the average heat transfer coefficient in the thin film zone, $h_{lt}(z)$, the meniscus radius, $r_c(z)$, and the local average heat transfer coefficient in the meniscus zone, $h_{lm}(z)$. As seen, the thin film zone width η_e decreases with increasing axial distance while the meniscus radius, $r_c(z)$, increases with z, so that the thin film zone becomes narrower while the corresponding meniscus zone becomes wider accordingly. This is primarily due to the fact that more steam is condensed and drained into the channel corners with steam flowing downstream. Fig. 5 also indicates that the average heat transfer coefficient in the meniscus zone, $h_{lm}(z)$, decreases monotonically with z, while the average heat transfer coefficient in the thin film zone, $h_{lt}(z)$, increases due to the decrease of the liquid film thickness.

The cross-sectional average heat transfer coefficients, $h_i(z)$, predicted by the present model are compared with the correlation by Soliman et al. [26] for steam condensing inside a round tube in Fig. 6. The comparison is made under the condition of $\Delta T_i = 6$ °C and $Re_{vi} = 4500$ and for the same hydraulic diameter of $D_h = 1.16$ mm, corresponding to the side length of $b = 2.0$ mm for the triangular channel. The heat transfer coefficients for the triangle channel are significantly higher than that for the round tube. This enhancement is attributed to the thinner liquid film along the sidewall in the triangular channel, which results from the surface tension by the meniscus variation in the corners of the channel. As the steam flows further downstream, the enhancement becomes less pronounced, where the liquid film becomes sufficiently thick and, in turn, the influence of surface tension fades away.

Fig. 7 presents the effects of the inlet Reynolds numbers and the inlet subcoolings on the profile of the

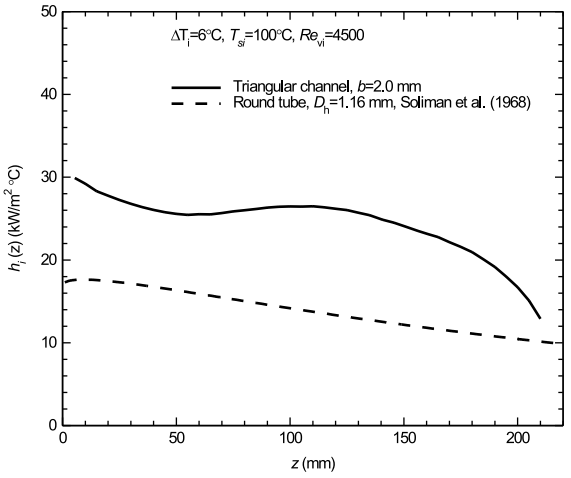

Fig. 6. Variations of the cross-sectional average heat transfer coefficients along the axial distance.

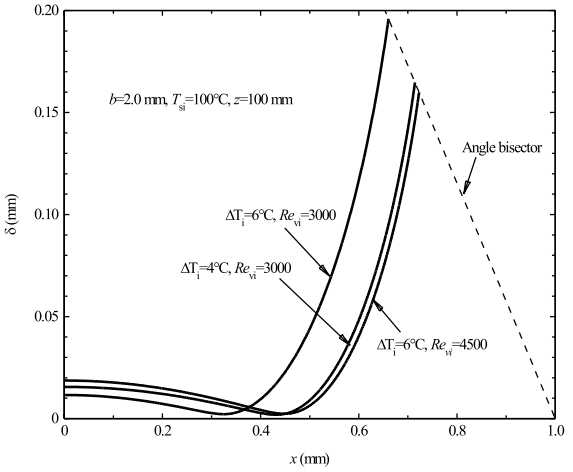

Fig. 7. Effects of inlet Reynolds numbers and inlet subcoolings on the liquid film thickness profiles.

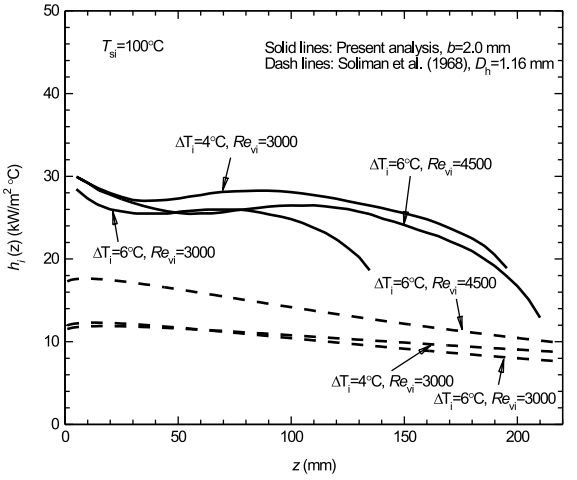

Fig. 9. Effects of inlet Reynolds numbers and inlet subcoolings on the cross-sectional average heat transfer coefficients.

liquid film thickness along the sidewall length. As indicated, an increase in the inlet Reynolds numbers (while keeping the inlet subcooling constant) or/and a decrease in the inlet subcooling (while keeping the inlet Reynolds number constant) yields a larger thin film zone or a smaller meniscus zone. As a result, the heat transfer coefficients for a smaller subcooling and a higher inlet steam velocity are higher than that for a larger subcooling and a lower inlet steam velocity, shown in Fig. 8.

The influences of inlet Reynolds numbers and inlet subcoolings on the cross-sectional average heat transfer coefficients, $h_i(z)$, are presented in Fig. 9. An increase in inlet steam velocity (represented by Re_{vi}) and a reduction in the inlet subcooling, ΔT_i, yields a higher heat transfer coefficient for both the triangular channel predicted here and the round tube correlation [26]. On the other hand,

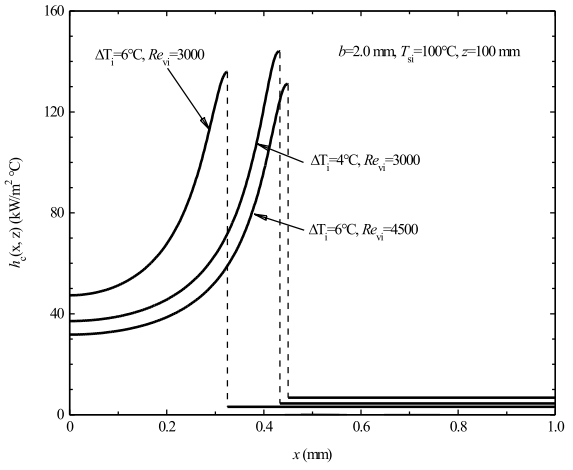

Fig. 8. Effects of inlet Reynolds numbers and inlet subcoolings on the local heat transfer coefficients along the sidewall.

a larger subcooling will lead to more steam to be condensed at each cross-section, making the thin film zone smaller and the liquid film thicker. At a constant condensing rate, a higher inlet steam velocity will exert a larger interfacial shear stress to reduce the meniscus zone, and to enlarge the thin film zone.

It can also be seen from Fig. 9 that the heat transfer coefficients for triangular channel are always substantially higher than that for the round tube having same hydraulic diameter with same inlet Reynolds number and same inlet subcooling. However, the heat transfer enhancements of the mini triangular channels with respect to the round tubes are quantitatively different for different cases. We define a heat transfer enhancement ratio as the ratio of the overall heat transfer coefficient of a triangle channel, defined by Eq. (56), to that of a round tube having same hydraulic diameter. It is found that the heat transfer enhancement ratio is 2.56 for Case I ($Re_{vi} = 4500$ and $\Delta T_i = 6$ °C), 2.99 for Case II ($Re_{vi} = 3000$ and $\Delta T_i = 6$ °C), and 3.47 for Case III ($Re_{vi} = 3000$ and $\Delta T_i = 4$ °C), respectively. A comparison between Cases I and II indicates that a larger inlet stream velocity leads to a smaller heat transfer enhancement ratio, i.e. the heat transfer enhancement of triangular channels becomes weaker for increasing inlet steam velocities. This can be explained as the heat transfer enhancement in triangle channels results from the capillary force induced by the sharp corners of the channels. However, a higher inlet velocity leads to a higher interfacial shear stress; more condensate is thus drained downward along the channel axis by the interfacial shear stress, as a result, the capillary effect induced by the sharp corners of the triangular channels becomes relatively weaker. A comparison between Cases II and III shows that a larger inlet subcooling yields a smaller heat transfer enhancement ratio. This is due to the fact

that a larger inlet subcooling leads to a higher condensation rate, causing flooding such that the meniscus zone becomes larger or the thin liquid film zone becomes smaller, the capillary effect becomes insignificant with the thin film zone shrinking in triangular channels.

The effect of the channel size (the sidewall length $b = 2.0$, 1.5, and 1.0 mm) on the cross-sectional average heat transfer coefficients, $h_i(z)$, is presented in Fig. 10 for $Re_{vi} = 3000$ and $\Delta T_i = 6$ °C. The smaller the channel size, the significantly higher heat transfer coefficients will be in the entry region. This is due to the fact that a smaller channel leads to a larger surface tension effect making the liquid film thickness thinner in the thin film zone. These behaviors can be seen in Figs. 11 and 12, where the profiles of the liquid film thickness and the local heat transfer coefficients at $z = 50$ mm and $z = 100$ mm are shown for different channel sizes. From Fig. 10, the cross-sectional average condensation heat transfer coefficients of the small channels decrease more rapidly with the increase of the axial distance z, as compared with that for larger channels. This can be is explained as follows. With the reduction of steam along the axial distance, the thin liquid film zone becomes relatively smaller, whereas the meniscus zone becomes larger, accordingly. However, for the small channels, the meniscus zone increases more rapidly with the axial distance, due to a higher condensation rate for the small channels in the entry region, shown in Figs. 11 and 12.

Fig. 10 indicates also that, the heat transfer coefficients for triangular channel are always substantially higher than that from correlation for round tube [26]. However, the heat transfer enhancement ratios of the mini triangular channels is 2.99 for the channel with $b = 2.0$ mm, 3.09 for the channel with $b = 1.5$ mm, and 3.56 for the channel of $b = 1.0$ mm.

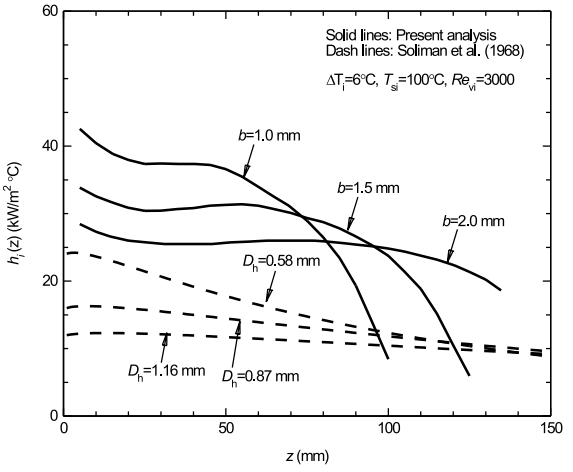

Fig. 10. Effects of the channel sizes on the cross-sectional heat transfer coefficients along the channel axial distance.

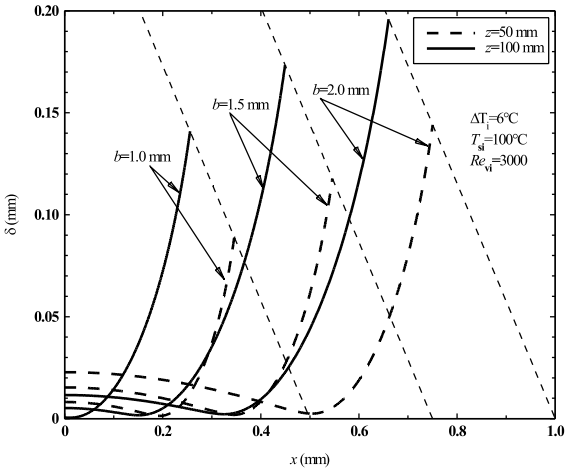

Fig. 11. Predicted effects of the channel sizes on the liquid film thickness profiles.

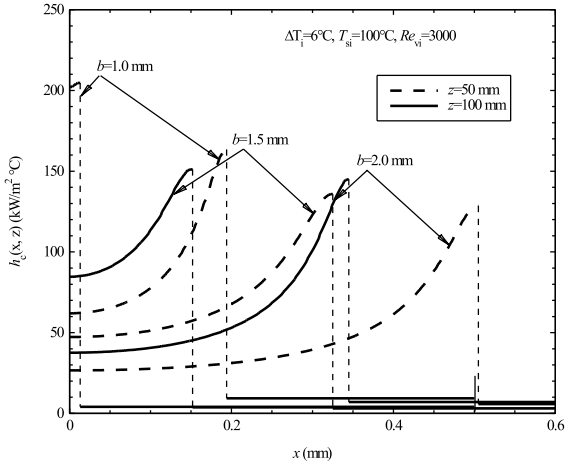

Fig. 12. Predicted effects of the channel sizes on the local heat transfer coefficient along the sidewall.

3.2.3. Two-phase pressure drops

Fig. 13 presents the variations of the two-phase pressure drops in both the mini triangular channel predicted and the round tube correlation [26] along the axial distance for Cases I, II, and III. In the entry region, the pressure drops in the mini triangular channels are close to those in the round tube for fixed inlet Reynolds number, Re_{vi}, inlet subcooling, ΔT_i, and hydraulic diameter. However, the pressure drops in the triangular channels decrease with increasing axial distance more rapidly. As indicated in Fig. 9, the condensation heat transfer coefficients of the triangular channels are larger than those of the round tubes at a fixed Re_{vi}, ΔT_i, and hydraulic diameter, larger condensation heat transfer coefficient leads to a larger condensing rate and thus, a

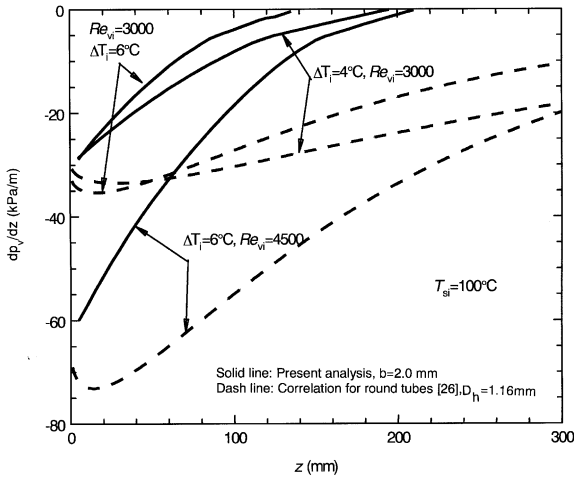

Fig. 13. Two-phase pressure drops at various vapor inlet velocities and for different inlet subcoolings.

quicker reduction in the steam velocity along the axial distance, the pressure drops in the triangular channels decrease more rapidly. As seen in Fig. 13, a larger inlet subcooling, ΔT_i, and a lower inlet Reynolds number, Re_{vi}, yield lower two-phase pressure drops in both the triangular and the round channels.

The two-phase pressure drops in the triangular channels with side lengths of 2.0, 1.5, and 1.0 mm under the condition of $Re_{vi} = 3000$ and $\Delta T_i = 6$ °C are plotted in Fig. 14, from which the two-phase pressure drop increases with decreasing channel size. This is attributed to the fact that for the same inlet Reynolds number, the steam velocity will be higher in a smaller channel, leading to a larger interfacial shear stress.

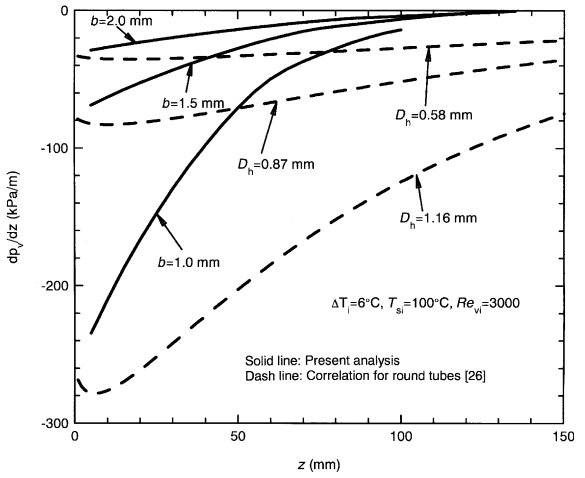

Fig. 14. Effects of the channel sizes on the two-phase pressure drops.

4. Concluding remarks

An analytical model for predicting film condensation of vapor flowing inside a vertical mini triangular channel under the influence of a superimposed pressure has been presented. The analysis is made by dividing the field of the liquid–vapor concurrent two-phase flow through the triangular-shaped cross-section into the three zones: the thin liquid film flow on the sidewall, the condensate flow in the corners, and the vapor core flow in the center. A number of important effects including the capillary force induced by the free liquid film curvature variation, the interfacial shear stress, the interfacial thermal resistance, the gravity, the axial pressure gradient, and the saturation temperatures have been incorporated in the model. The analyses show that, the cross-sectional average heat transfer coefficients of steam condensing inside a triangular channel are substantially higher than that inside a round tube with same hydraulic diameter, especially in the entry region. Reduction in channel sizes leads to higher heat transfer coefficients in the entry region. However, the heat transfer coefficient decreases with increasing z more rapid for smaller channels. In addition, it is found that the condensation enhancement of the triangular channels, with respect to that of the round tubes with the same hydraulic diameter, becomes more significant as the channel size, the inlet steam velocity, and the inlet subcooling decreased.

Acknowledgements

This work was supported by Hong Kong RGC Earmarked Research Grant No. HKUST 6178/00E.

References

[1] L.A. Guntly, N.F. Costello, US Patent No. 4998580, 1991.
[2] C.Y. Yang, R.L. Webb, Condensation of R-12 in small hydraulic diameter extruded aluminum tubes with and without micro-fins, Int. J. Heat Mass Transfer 39 (1996) 791–800.
[3] C.Y. Yang, R.L. Webb, A predictive model for condensation in small hydraulic diameter tubes having axial microfins, ASME J. Heat Transfer 119 (1997) 776–782.
[4] W.W. Akers, H.A. Deans, O.K. Crosser, Condensation heat transfer within horizontal tubes, Chem. Engrg. Symp. Series 55 (1959) 171–176.
[5] B.X. Wang, X.Z. Du, Condensation on the outside surface of a small/mini diameter tube for vapor flowing through a horizontal annulus surround by an adiabatic concentric tube, Int. J. Heat Mass Transfer 43 (2000) 1391–1398.
[6] S. Nozu, H. Honda, Condensation of refrigerants in horizontal, spirally grooved microfin tubes: numerical analysis of heat transfer in the annular flow regime, ASME J. Heat Transfer 122 (2000) 80–91.

[7] V.A. Karkhu, V.P. Borovkow, Film condensation of vapor at finely-finned horizontal tubes, Heat Transfer-Soviet Res. 6 (1971) 76–83.
[8] V.G. Rifert, P.A. Barabash, A.B. Goluboev, G.G. Leont'yev, S.I. Chaplinskiy, Investigation of film condensation enhanced by surface forces, Heat Transfer-Soviet Res. 9 (1977) 23–27.
[9] S. Hirasawa, K. Hijikata, Y. Mori, W. Nakayama, Effect of surface tension on condensate motion in laminar film condensation (study of liquid film in a small trough), Int. J. Heat Mass Transfer 23 (1980) 1471–1478.
[10] Y. Mori, K. Hijikata, S. Hirasawa, W. Nakayama, Optimized performance of condensers with outside condensing surfaces, ASME J. Heat Transfer 103 (1981) 96–102.
[11] T. Adamek, R.L. Webb, Prediction of film condensation on vertical finned plates and tubes: a model for the drainage channel, Int. J. Heat Mass Transfer 33 (1990) 1737–1749.
[12] D. Khrustalev, A. Faghri, Thermal analysis of a micro heat pipe, ASME J. Heat Transfer 116 (1994) 189–198.
[13] Y. Zhang, A. Faghri, Numerical simulation of condensation on a capillary grooved structure, Numer. Heat Transfer Part A 39 (2001) 227–243.
[14] S.K. Thomas, R.C. Lykins, K.L. Yerkes, Fully developed laminar flow in trapezoidal grooves with shear stress at the liquid–vapor interface, Int. J. Heat Mass Transfer 44 (2001) 3397–3412.
[15] V.P. Carey, Liquid–Vapor Phase-Change Phenomena: An Introduction to the Thermophysics of Vaporization and Condensation Processes in Heat Transfer Equipment, Hemisphere, Washington, DC, 1992.
[16] P.C. Stephan, C.A. Busse, Analysis of the heat transfer coefficient of grooved heat pipe evaporator walls, Int. J. Heat Mass Transfer 35 (1992) 383–391.
[17] C.Y. Wang, M. Groll, S. Rösler, C.J. Tu, Porous medium model for two-phase flow in mini channels with applications to micro heat pipe, Heat Recovery & CHP 14 (1994) 377–389.
[18] A.E. Saez, R.G. Carbonell, Hydrodynamic parameters for gas–liquid cocurrent flow in packed beds, AIChE J. 31 (1985) 52–62.
[19] X. Xu, V.P. Carey, Film evaporation from a micro-grooved surface-an approximate heat transfer model and comparison with experimental data, AIAA J. Thermophys. Heat Transfer 4 (1990) 512–520.
[20] J.P. Longtin, B. Badranand, F.M. Gerner, A one-dimensional model of a micro heat pipe during steady-state operation, ASME J. Heat Transfer 116 (1994) 705–709.
[21] G.P Peterson, H.B. Ma, Theoretical analysis of the maximum heat transport in triangular grooves: a study of idealized micro heat pipes, ASME J. Heat Transfer 118 (1996) 731–739.
[22] M.J. Ha, G.P. Peterson, The interline heat transfer of evaporating thin films along a micro grooved surface, ASME J. Heat Transfer 118 (1996) 747–754.
[23] A. Bejan, in: Convective Heat Transfer, Wiley, New York, 1984, pp. 77–78.
[24] A.E. Dukler, Fluid mechanics and heat transfer in vertical falling film systems, Chem. Engrg. Prog. Symp. Series 30 (56) (1960) 1.
[25] I.Y. Chen, G. Kocamustafaogullari, Condensation heat transfer studies for stratified, cocurrent two-phase flow in horizontal tubes, Int. J. Heat Mass Transfer 30 (1987) 1133–1148.
[26] M. Soliman, J.R. Schuster, P.J. Berenson, A general heat transfer correlation for annular flow condensation, ASME J. Heat Transfer 90 (1968) 267–276.